Chinese Journal of Aeronautics, (2014),27(2): 189–199

Chinese Society of Aeronautics and Astronautics
& Beihang University

Chinese Journal of Aeronautics

cja@buaa.edu.cn
www.sciencedirect.com

Progress in helicopter infrared signature suppression

Zhang Jingzhou *, Pan Chengxiong, Shan Yong

Jiangsu Province Key Laboratory of Aerospace Power System, College of Energy & Power Engineering, Nanjing University of Aeronautics and Astronautics, Nanjing 210016, China

Received 24 April 2013; revised 4 November 2013; accepted 10 December 2013
Available online 19 February 2014

KEYWORDS

Helicopter;
Infrared radiation;
Infrared suppression;
Internal aerodynamics;
Mixer-ejector

Abstract Due to their low-attitude and relatively low-speed fight profiles, helicopters are subjected to serious threats from radio, infrared (IR), visual, and aural detection and tracking. Among these threats, infrared detection and tracking are regarded as more crucial for the survivability of helicopters. In order to meet the requirements of infrared stealth, several different types of infrared suppressor (IRS) for helicopters have been developed. This paper reviews contemporary developments in this discipline, with particular emphasis on infrared signature suppression, advances in mixer-ejectors and prediction for helicopters. In addition, several remaining challenges, such as advanced IRS, emissivity optimization technique, helicopter infrared characterization, etc., are proposed, as an initial guide and stimulation for future research. In the future, the comprehensive infrared suppression in the 3–5 μm and 8–14 μm bands will doubtfully become the emphasis of helicopter stealth. Multidisciplinary optimization of a complete infrared suppression system deserves further investigation.

1. Introduction

Helicopters play important roles in air-to-ground fire covering and short-distance air-to-air fights, as well as battlefield force transferring and anti-tank missions. Due to their low-attitude and relatively low-speed fight profiles, helicopters are subjected to serious threats from radio, infrared (IR), visual, and aural detection and tracking. Among these threats, infrared detection and tracking are regarded as more crucial for the survivability of helicopters. Firstly, passive detection and tracking by infrared signature seeking missiles are tactically superior to active ones for a comparable detection range. Infrared seekers have exploited techniques to passively acquire and intercept airborne targets by detecting their infrared emitting energy. Developments in infrared detection and tracking have increased the effectiveness of infrared-guided missiles, which are now portable and have proliferated world-wide. The rapid advances in processor and detector array technology have led to enhanced sensitivity, low noise, multi-spectral, and smart detection capabilities.[1–3] On the other hand, with the increase of the ratio of power to weight for turbo-shaft engines mainly equipped in helicopters, the exhaust temperature increases tremendously, resulting in an infrared signature augment intensively. Consequently, infrared signature suppression is an important issue associated with helicopter susceptibility.

This paper reviews contemporary developments in this discipline, with particular emphasis on infrared signature suppression and prediction from helicopters. In addition,

* Corresponding author. Tel.: +86 25 84895909.
E-mail address: zhangjz@nuaa.edu.cn (J. Zhang).

Peer review under responsibility of Editorial Committee of CJA.

Production and hosting by Elsevier

1000-9361 © 2014 Production and hosting by Elsevier Ltd. on behalf of CSAA & BUAA. Open access under CC BY-NC-ND license.
http://dx.doi.org/10.1016/j.cja.2014.02.007

several remaining challenges are proposed, as an initial guide and stimulation for further research.

2. Sources of infrared signature

The sources of infrared signature in a helicopter and their classification are shown in Fig. 1. The important internal infrared sources include plume emission and surface emissions from the following: (a) engine hot parts, (b) exhaust plume, and (c) airframe skin heated by the engine and plume. Besides, the reflected skyshine, earthshine, and sunshine contribute to the total infrared signature.

The attenuation of infrared radiation in the atmosphere is highly dependent on wavelength of radiation, temperature, and composition of radiation participating gases. Mainly two atmospheric windows (3–5 μm and 8–14 μm) are used for surveillance and tracking where the transmittance is high. Tailpipe is the major and reliable source for infrared signature level in the 3–5 μm band because of the large amount of heat produced by combustion inside the gas turbine engine. The helicopter rear fuselage skin is always heated by the flow of hot combustion products in the embedded engine. Though the spectral radiance of the rear fuselage is less than that of the tailpipe, infrared emission from the rear fuselage is important especially in the 8–14 μm band. Meanwhile, the solid angle subtended by the rear fuselage skin is an order of magnitude larger than that of the tailpipe. Unlike surfaces of solids, gases emit and absorb radiation only at discrete wavelengths associated with specific rotational and vibrational frequencies. These frequencies depend on the particular type of molecules, temperature, pressure, and molecular concentration of radiation participating species. In general, the infrared signature level from the plume is much less significant than those from the tailpipe and the rear fuselage skin, especially in the 8–14 μm band.[4]

Thompson et al.[5] presented the infrared signature breakdown of a Bell-205 (UH-1H) helicopter in the 3–5 μm band, as shown in Fig. 2. The signature values shown in this figure were predicted using the infrared signature modeling software developed by DAVIS. The largest contributor to the helicopter infrared signature is the direct view of the 600–700 °C power turbine stages. The next signature component of importance is the hot tailpipe metal. Visible up to 120° off-tail, the tailpipe metal provides a strong target for infrared-guided missiles for all views from behind the helicopter. It is also shown that the

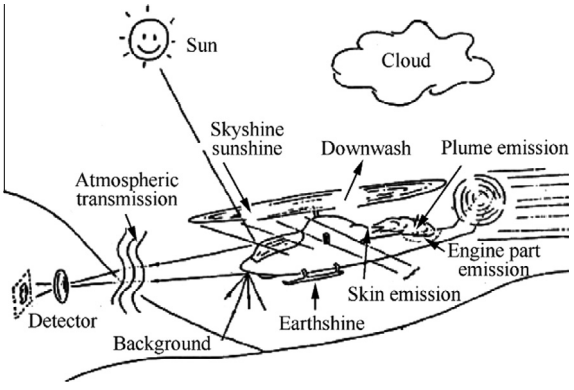

Fig. 1 Sources of infrared signature in a helicopter and their classification.

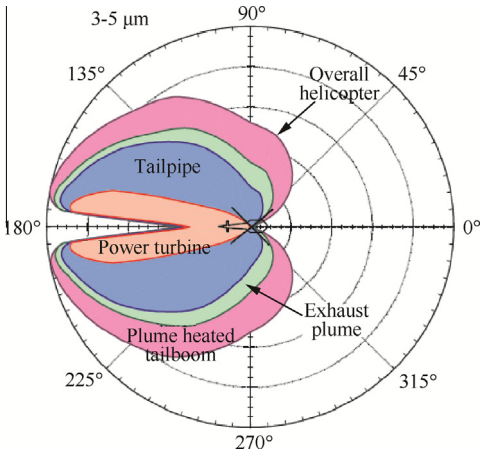

Fig. 2 Infrared signature variation of a Bell UH-1H helicopter.[5]

engine exhaust plume is the least contributor, followed by the tail boom heated by the plume. When viewed from the front and sides, the plume and the airframe contribute, and when viewed from the rear, the engine hot parts become the major source of infrared radiation.

3. Advances in infrared suppressors

The first generation of infrared suppressors (IRSs) for helicopters typically features an upward-bend nozzle shielded from a direct view by an insulating cowl. It is generally regarded as being adapted for opposing infrared-guided missiles working at the 1.7–2.8 μm band. While this principle holds for radiation of any wavelength, new warheads operating in the 3–5 μm band have the additional capability of locking on weaker signals emitted at relatively lower temperatures. The exhaust plume radiates a detectable amount of energy due to discrete rays in the carbon dioxide spectrum in the 3–5 μm band. Diluting the engine plume with cold ambient air decreases CO_2 concentration and temperature and therefore reduces the target detectability. This is most conveniently achieved by means of a passive ejector as has been widely recognized. When the primary jet mixes out to fill the larger area cross-section of the mixing duct, the turbulent shear layer entrains a secondary flow into the mixing duct to dilute the primary flow. Based on this mechanism, several different types of IRS for helicopter engines have been developed, such as cascaded ejector-based IRS, black hole ocarina (BHO) IRS, lobed mixer-ejector IRS, etc.[6–8]

3.1. BHO IRS

The BHO system used on the YAH-64 Apache helicopter is a low-cost IR suppressor[6] without any moving part, as seen in Fig. 3. In Fig. 3, θ denotes the azimuthal angle, R_I is relative infrared intensity. Known as the "black hole" infrared suppression system, the principle revolves around directing the engine exhaust through special ducts which combine the efflux with the air-stream passing over the aircraft. The air-stream thus dissipates the hot exhaust that emerges from the vents evenly, rather than allowing hot spots to appear. Prior to exit, the temperature is further reduced from 574 °C to 304 °C. The engine exhaust ports are angled outward from the airframe to better direct the output into the air-stream. Secondary vents

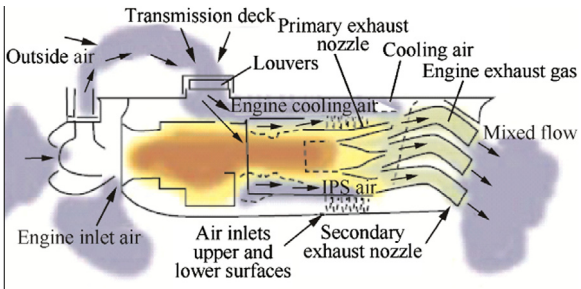

(a) Schematic of a BHO suppressor

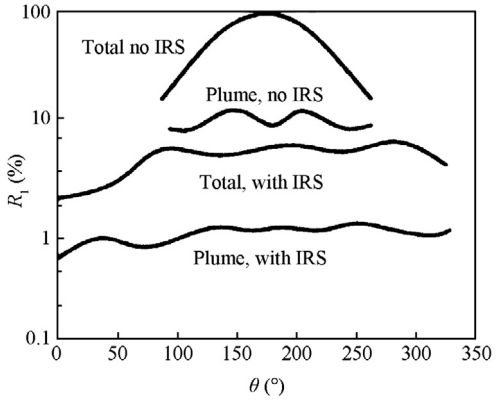

(b) IR signature with or without a BHO suppressor

Fig. 3 BHO suppressor.[6]

along the upper surface of the outlets help to dissipate the heat by diverting part of the emissions into the flow along the top of the airframe. To further reduce the infrared signature of the aircraft, exhaust output is used to draw in fresh air in order to cool both the engines and the transmission, the latter's cooling being assisted through oil heat exchangers.

Bettini et al.[9] conducted analysis of the fluid-dynamic performance of a complete IRS system for a helicopter engine, assuming the coupling of the infrared suppression system to the Rolls-Royce MK 1004 turbo-shaft engine that equips the Mangusta A129 light-attack helicopter. An important effect introduced by the infrared suppression configuration is the mixing of the hot exhaust gases with fresh ambient air. The external surface of the masking box has a high porosity that allows the suction of external air into the suppression system using the ejector effect of the high-speed internal mainstream of the hot gases. The porosity of the masking box's external surface is obtained by a high number of louvers (more than 18000) as sketched in Fig. 4. Each louver has an open air height of only 0.5 mm.

3.2. Lobed mixer-ejector IRS

Fig. 5 shows the lobed mixer-ejector IRS adopted by Turbomeca Dauphin SA365C.[7] In Fig. 5, θ denotes the azimuthal angle, R_1 is relative infrared intensity. Evaluation tests showed that this kind of infrared suppressors was of high dilution, low turbine backpressure, low aerodynamic drag, compactness, and light weight. It reduced infrared signal/noise ratio in the 3–5 μm band by 39 dB, with an acceptable power loss limited in 2.5% at hover IGE power.

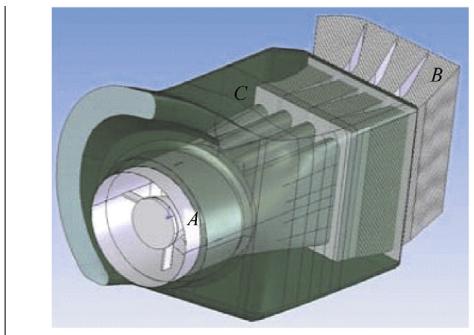

A—Nozzle box;*B*—Masking box;*C*—Conveyor for ambient air

(a) Schematic of the suppressor

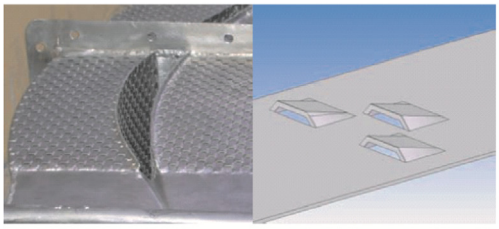

(b) Masking box surface and louvers

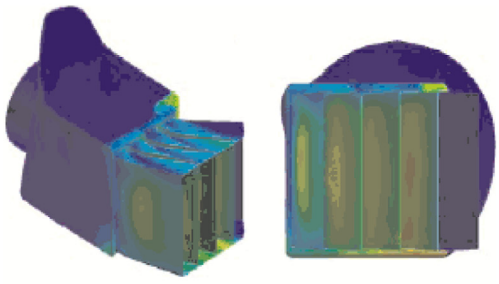

(c) Static temperature contours

Fig. 4 Infrared suppression system.[9]

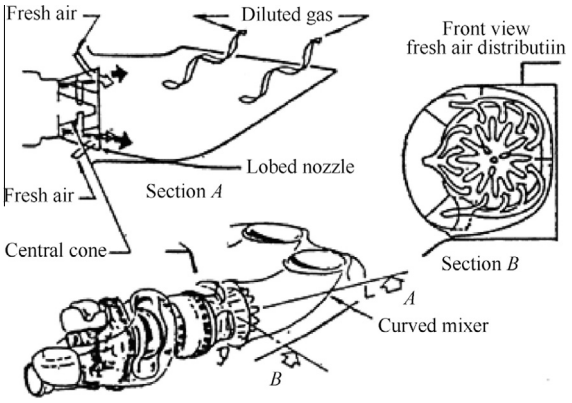

Fig. 5 Infrared suppression system used in SA365C.[7]

Zhang et al.[10–14] made a series of fundamental studies on a lobed nozzle mixer-ejector IRS for helicopter exhaust systems. Fig. 6 presents the relationship between infrared intensity and azimuthal angle for the lobed mixer-ejector IRS. A comprehensive summary on the lobed nozzle mixer-ejector infrared signature suppressor was made by Zhang et al.[12] The effects of ambient air pumping-mixing and heat shelter-insulation

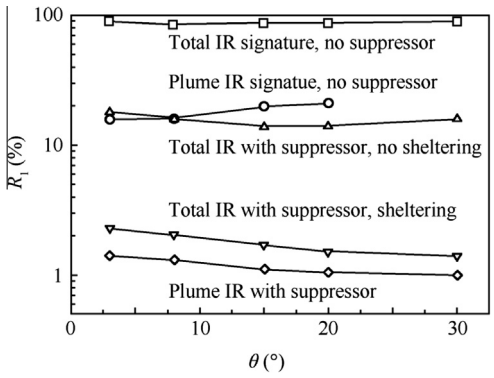

Fig. 6 Relative infrared intensity vs azimuthal angle.[12]

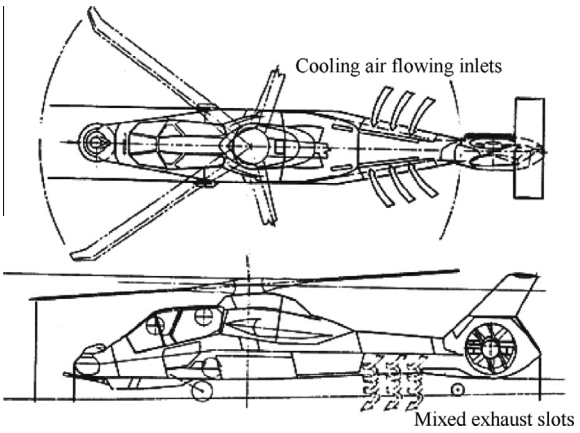

Fig. 7 Comanche IRS.[17]

on decreasing the target infrared signature and the infrared signature similarity between two scaled models with different scale factors were concluded: (a) ambient air pumping-mixing plays a dual role for reducing both the exhaust and mixing duct temperatures and this role is more obvious in the case of a larger mass flow ratio of secondary flow to primary flow. Sheltering from the hot mixing duct wall makes the sheltering sheath temperature close to ambient temperature in case of the sheltering distance greater than 20 mm; (b) ambient air pumping-mixing contributes about 85% suppression for the total target infrared radiation intensity and heat shelter-insulation contributes about 10% suppression; (c) while the primary flow velocity, temperature, and pressure are the same for different scaled models, the irradiances for different scaled models are almost the same and the infrared radiation intensity is almost proportional to the square of the model scale factor.

3.3. IRS embed inside helicopter rear airframe

Boeing-Sikorsky RAH-66 Comanche is the first helicopter developed specifically for a low-observable stealth role.[15,16] To reduce the radar cross-section, the all-composite fuselage sides are flat and canted, and rounded surfaces are avoided by use of faceted turret and engine covers. It is reported that the Comanche will be able to approach five times closer to an enemy's radar than a YAH-64 Apache helicopter without being detected. The advanced rotor design permits operation at low speed, allowing the Comanche to sneak 40% closer to a target than the Apache, without being detected by an acoustical system. The Comanche is the first helicopter in which the infrared suppression system is integrated into the airframe, as seen in Fig. 7. This innovative Sikorsky design feature provides IRSs that are built into the tail-boom, providing ample length for complete and efficient mixing of engine exhaust and cooling air flowing through inlets above the tail. The mixed exhaust is discharged through slots built into an inverted shelf on the sides of the tail-boom. The gases are cooled so thoroughly that a heat-seeking missile cannot find and lock on the Comanche. The Comanche only radiates 25% of the engine heat of current helicopters.

Utilizing a ground test model, an experimental diagnostic study on the infrared suppressor integrating the exhaust system with the tail part of a helicopter has been performed by Tang et al.[17,18] to investigate the effects of ambient air pumping-mixing and rotor downwash on reducing the exhaust system temperature and diminishing the target infrared signature. The result shows that the gas temperature can be reduced by at least 50% by a lobed nozzle which injects ambient air to mix with the hot gas; and rotor downwash flow that cools the tail part of the model can cause a decrease of total infrared radiation between 3–5 μm and 8–14 μm equivalent to about 39% and 33%.

4. Advances in mixer-ejectors

Passive mixer-ejector is the key element in an infrared suppressor for helicopters. In short efficient mixer-ejector systems, the primary nozzle plays an important role on pumping and mixing capacities. A lobed nozzle is illustrated to be one of the best choices for the primary nozzle.[19,20]

4.1. Mechanism of mixing enhancement

The concept of the lobed nozzle is oriented from the lobed or forced mixer which is firstly used in a turbofan engine to mix bypass flow and core flow in a short distance. Early research by Paterson,[21] Povinelli and Anderson[22] indicated that large-scale secondary flows, not viscous diffusion, were the key to low-loss efficient mixing. The forced lobes used the third dimension to initiate large-scale streamwise vortices which stirred co-flowing streams of fluid together providing convective mixing rather than shear mixing. The streamwise vortices were reported to interact within a small distance downstream from the mixer trailing edge, but remain the largest-scale flow structure for three to ten lobe wavelengths downstream. Further investigations on the fundamental mechanism of mixing enhancement were carried out either experimentally or numerically by a lot of researchers.[23–26] The fundamental features of the flow development downstream from a lobed mixer were explained by McCormick and Bennett[24] and shown schematically in Fig. 8. Small-scale periodic vortex structures, known as the normal vortices, are generated in the strong free shear layer shedding from the trailing edge of the lobed mixer, due to the Kelvin–Helmholtz instability promoted by the inflectional velocity profile of the shear layer. These normal vortices

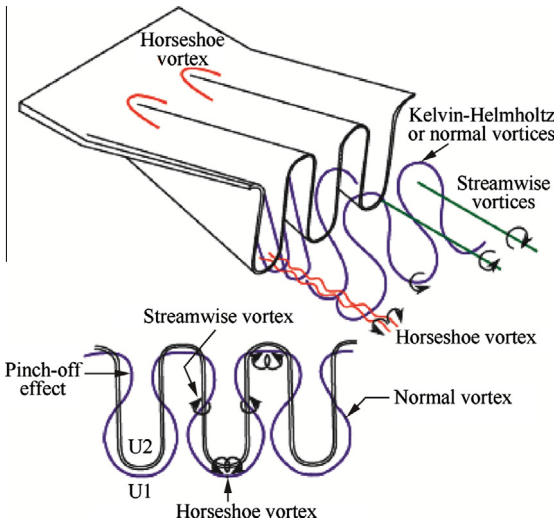

Fig. 8 Schematic of vortical structures downstream from a lobed mixer.[24]

are continuously connected along the perimeter of the convoluted free shear layer. The contour of these normal vortices is deformed by the streamwise vortices so that the normal vortices are eventually pinched off and broken down, resulting in high levels of turbulent mixing followed by their breakdown into small-scale turbulent structures. Furthermore, the existence of a counter-rotating streamwise vortex pair within the troughs of the lobes is also commonly observed downstream from the discharge plane, which are the legs of horseshoe vortices that are developed as the upstream wall boundary layer is wrapped around the lobe peaks.

4.2. Advanced lobed-mixers

The strength of streamwise vortices depends primarily on the lobe geometry. Early preliminary investigations[27,28] were mainly focused on estimating the influences of geometric parameters on the performance of forced exhaust mixers including the number of lobes, lobe radial penetration angles, lobe shape and length, etc. Results from these studies provided a data base for optimizing the design of turbofan forced mixer exhaust systems.

Skebe et al.[29] noted that sinusoidally shaped lobes tended to produce lower secondary flow velocities and mix less efficiently than those with a geometry of parallel lobe sidewalls due to the merger of sidewall boundary layers in the troughs of the former geometry. Yu et al.[30] made velocity and turbulence characteristics measurements downstream from a lobed forced mixer with three different trailing edge configurations using a two-component laser-Doppler anemometer. The three trailing edge configurations under investigation had the shapes of a square wave, a semi-circular wave, and a triangular wave. Measurements indicated that the strength of the secondary flow shed by a lobe was not the only parameter which determined the effectiveness of mixing. The boundary layer thickness which grew along the side-walls of the lobe penetration and the subsequent shedding of the boundary layer to the wake region were of equal importance.

Recently, some research was conducted for advancement of the lobed mixer contour, such as scalloping and scarfing of the lobes, lobe deflection, flow swirling, etc. Yu[31] and Mao[32] et al. compared scalloped and unscalloped planar mixers with the same penetration angle and trailing edge profiles. They showed that the streamwise vorticity was enhanced and its decay rate accelerated in scalloped mixers, largely because of the formation of two pairs of streamwise vortices at each lobe. They also reported lower losses for scalloped mixers, compared with other configurations, possibly due to their lowest wetted surface area within the penetration region. Salman et al.[33] made a computation for prediction of a non-isothermal three-dimensional mixing layer created by a scarfed lobed mixer. Results showed that the scarfed mixer introduced strong flow asymmetries in the azimuthal direction. This caused adjacent vortical structures produced by the alternating short and long gullies of the lobes to interact with one another and this behavior dominated the flow evolution. Nastase and Meslem[34] conducted an experiment on vortex dynamics and mass entrainment in turbulent lobed jets with and without lobe deflection angles. Two turbulent 6-lobed air jets with and without lobe deflection angles were studied experimentally and compared with a reference circular jet having the same initial Reynolds number. In the potential core region, the jet with inclined lobes displayed a superior entrained flow rate reaching up to four times the value of the circular jet while the jet with straight lobes displayed a maximum gain of 70%. The comparison of the mean and instantaneous vorticity fields showed that the lobe inclinations organized the cross flow and amplified its shear. Lei et al.[35] explored the effects of core flow swirl on the flow characteristics of a scalloped forced mixer. At low swirl angles, additional streamwise vortices were generated by the deformation of normal vortices due to the scalloped lobes. With increased core swirl, greater than 10°, additional streamwise vortices were generated mainly due to radial velocity deflection, rather than stretching and deformation of normal vortices. At high swirl angles, stronger streamwise vortices and rapid interaction between various vortices promoted downstream mixing. Mixing was enhanced with minimal pressure and thrust losses for inlet swirl angles less than 10°.

4.3. Parameters on mixer-ejector performances

The use of lobed mixers in short efficient systems was firstly presented by Presz et al.[19] They conducted an experimental study to investigate the benefits of using forced mixer lobes in low-pressure ratio, ejector/diffuser systems. Their results showed over a 100% increase in both pumping and thrust augmentations when compared with conventional ejector designs. The test results also indicated that forced mixer lobes resulted in nearly complete mixing in very short ejector duct lengths and allowed the use of aggressive diffuser designs without resulting in stall.

Skebe et al.[36] made experimental investigations of the effects of geometric and operating parameter variations, such as the lobe penetration angel and height, the mixing duct diameter and length, the diffuser expand angle, pressure ratio, etc., on the mixer-ejector pumping performance of a representative low-pressure ratio jet engine exhaust system. Their results suggested guidelines for designing mixer-ejector geometries to achieve optimum pumping efficiency. From the view of jet momentum utilization, they presented three primary jet spread regimes, as seen in Fig. 9. For the ‘‘under-utilized’’ condition,

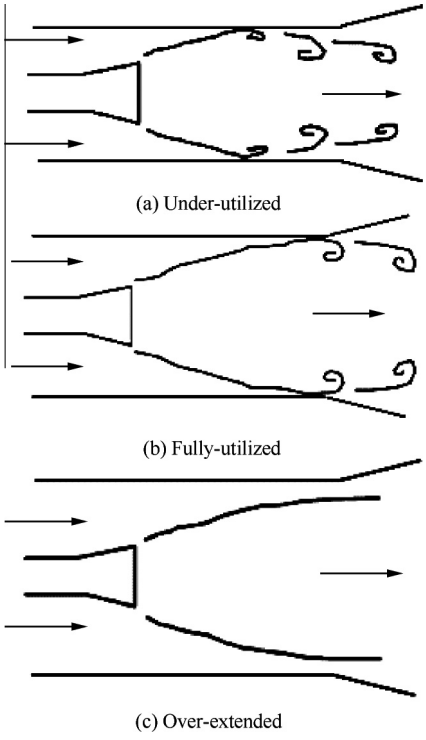

Fig. 9 Schematic of primary jet spread.[36]

after departing the mixer lobes, the high-momentum primary flow pre-maturely interacted with the mixing duct walls, limiting its potential entrainment surface and causing it to reflect back and incur high viscous losses through self-mixing. When operated in its "fully-utilized" condition, with which highest performance levels were achieved due to the primary flow momentum entrainment surface reaching its fullest extent just upon its interaction with the duct walls, large diffusion angles could be similarly maintained with a slight decrease in ejector performance. For the "over-extended" condition, the high-momentum primary core did not reach the duct walls and was unable to accelerate the entire duct flow, resulting in reduced pumping as well as poor diffusion and duct pressure recovery.

These suggested guidelines were confirmed by Zhang[37] and Liu[38] et al. Liu[39] also made an experimental and numerical investigation on a circularly lobed nozzle with/without a central plug. Results showed that the central plug increased the pumping ratio about 60%–70% and the total pressure prior to flow entry into the circularly lobed nozzle increased about 0.8%–1.0% over one without a central plug.

For the mixer-ejector with curved mixing duct, the impingement of the primary flow on the curved wall causes an increase of the static pressure near the wall and the interior of the mixing duct, and the pumping ratio is reduced. The curved angle of the mixing duct is the most significant factor on the pumping ratio. The pumping ratio is rapidly reduced with the increase of the curved angle. The thermal mixing efficiency is also sharply reduced when the angle exceeds 40°, as seen in Fig. 10.[40] Here, D, L and β denote the diameter, length and curved angle of the mixing duct, respectively.

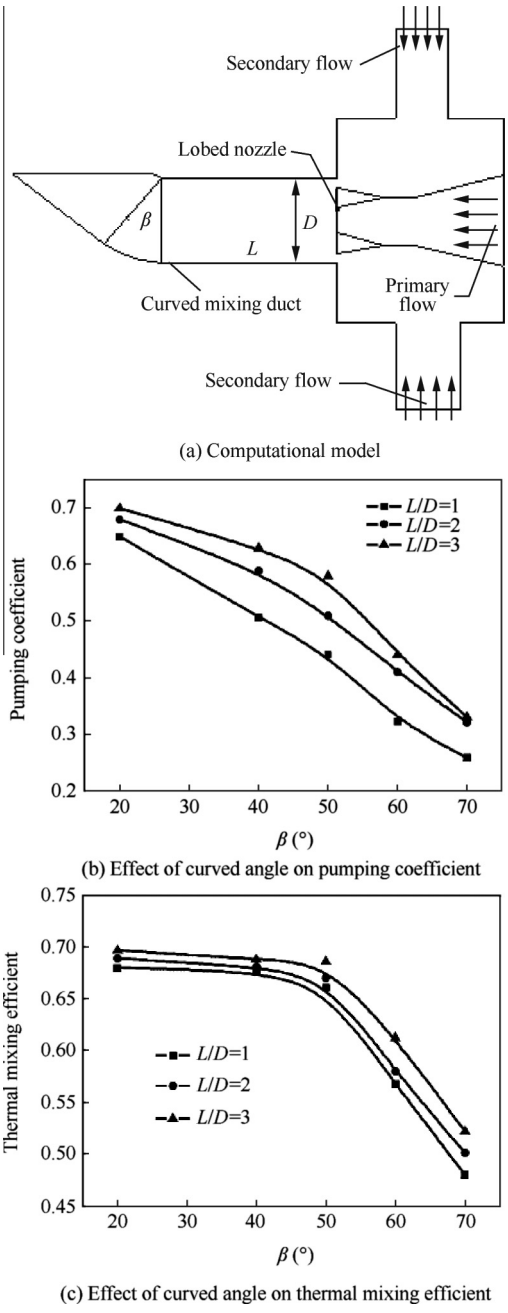

Fig. 10 Lobed mixer-ejector with curved mixing duct.[40]

5. Several remaining challenges

Helicopter infrared suppression technology meets very advanced requirements today, but it is also true that it has reached a plateau, for the most part, with further increases in suppressing efficiency, coming as incremental improvements rather than revolutionary changes. In the interim period, advancements in helicopter infrared signature suppression technology have primarily been in more detailed understanding of infrared sources and higher sophistication of analytical tools. Having reached this plateau, there are several questions to be considered in pushing infrared suppression technology further.

5.1. Advanced IR suppressor

In response to the rapid development of infrared detector technology, a generic set of requirements has been assembled to drive advanced IRS designs:

(1) An IRS must provide protection in all the potential threat wavebands.
(2) The IRS should not significantly increase the radar cross-section of the helicopter.
(3) The vehicle power loss associated with the combination of IRS pressure loss, weight, and induced aircraft drag must not significantly compromise operational effectiveness.
(4) The IRS must have reliability levels comparable with the remainder of the powerplant, with no additional action required outside existing maintenance periods.
(5) The cost of ownership of the system must be low in order to be compatible with helicopter operations. In particular, the non-recurring costs associated with system development must be minimized.

Ponton and Warnes[41] presented an acceptable provision of cooling flows and management of external aerodynamics. Particularly detailed analysis was carried out for the "fully integrated" Lynx/T800 configuration (see Fig. 11). This IRS installation draws plume dilution air from intakes mounted on both the "rear nacelle" and engine bays. Additional pressurized cooling flow (from the T800 inlet particle separator scavenge flow) is used to cool the plug's center body.

Presz and Werle[42] presented a patented suppressor, as seen in Fig. 12, which uses staggered lobes for more complete mixing, a two-stage ejector for higher diffusion rates, an efficient rounded first-stage ejector for engine matching, a turning shroud duct for line of sight blockage, and slanted lobes for faster mixing (STETS). The first-stage shroud transits from a round cross-section to a rectangular one to allow lobe staggering. Normally such exhaust duct area transition, line of sight blockage, and flow turning would generate significant losses which would cause backpressure effects on the jet engine. The STETS suppressor can dilute the hot jet exhaust, generate line of sight blockage, and provide secondary flow wall cooling while decreasing the backpressure on the jet engine.

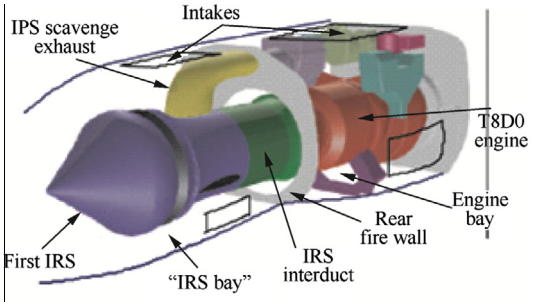

(a) Schematic of structure

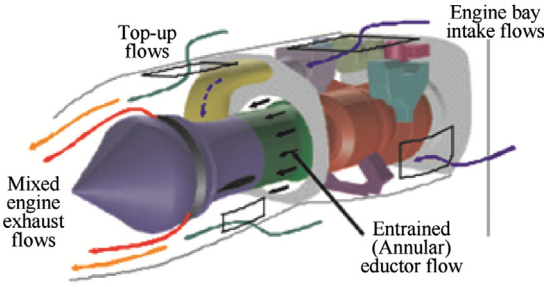

(b) Schematic of streamlines

Fig. 11 Schematics of the "fully integrated" Lynx/T800 FIRST IRS installation.[41]

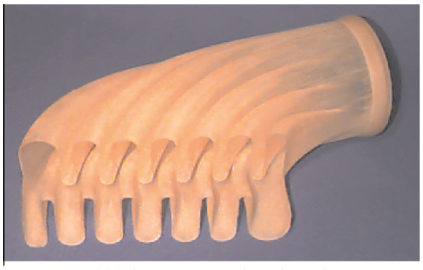

(a) First-stage turning shroud

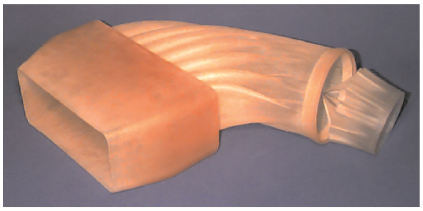

(b) Two-stage mixer-ejector

Fig. 12 Complete STETS suppressor model.[42]

5.2. Emissivity optimization technique

The rear fuselage skin is heated by the aero-engine embedded within it. One feasible technique for reducing the infrared signature level from a metallic surface is emissivity reduction or optimization. The emitted infrared radiation is a function of rear-fuselage skin temperature and emissivity. Thus, by altering these two parameters, infrared radiation emitted by a helicopter can be varied.

For a helicopter on a low-altitude mission, the infrared-guided threats come from two cases: against a surface-to-air missile (SAM) and against an air-to-air missile (AAM). Mahulikar et al.[43] made a preliminary investigation on assessing the applicability of the rear-fuselage-skin emissivity optimization technique for infrared signatures of low-flying aircraft. The effects of the rear-fuselage skin emissivity on the aircraft lock-on range (R_{LO}) and the missile infrared irradiance (H) are shown in Fig. 13. In this figure, ε_{fuse} denotes the rear-fuselage skin emissivity.

It is indicative that optimizing the rear-fuselage skin emissivity reduces the aircraft lock-on range significantly. In the 3–5 μm band, the rear-fuselage skin emissivity can be optimized to a nonzero value. In the 8–12 μm band, the rear-fuselage skin emissivity should be reduced to close to zero, for minimizing susceptibility against infrared-guided SAMs. In case of infrared-guided AAMs, there is a non-zero value of the rear-fuselage skin emissivity for which the infrared

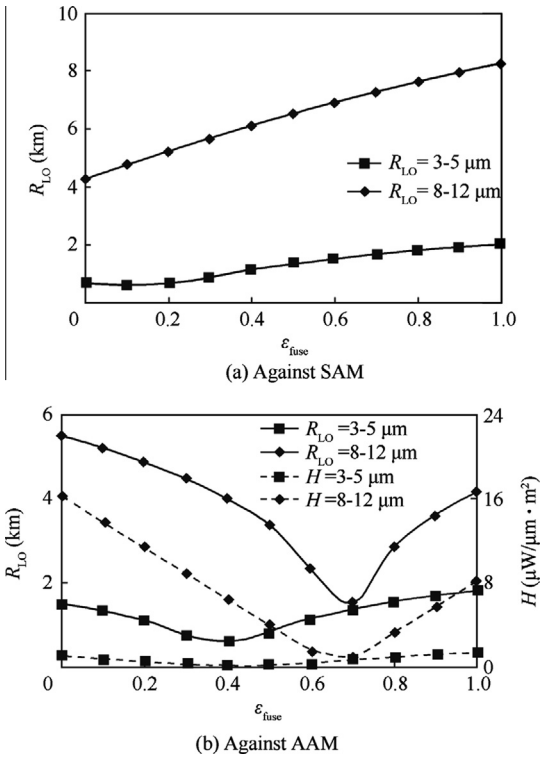

Fig. 13 Effects of rear-fuselage skin emissivity on aircraft lock-on range and missile infrared irradiance.[43]

signature level from the rear-fuselage skin is minimized. Earthshine reflected by the rear-fuselage skin is significant in dictating aircraft susceptibility to infrared-guided SAMs in the 8–12 μm band, but the role in the 3–5 μm band is insignificant. In the case against a SAM, the lower portion of the rear-fuselage skin is visible to the SAM. In the case of an AAM, the side portion of the rear-fuselage skin is visible. Therefore, different parts of the rear-fuselage skin should have different emissivity, for minimizing its infrared signature level against infrared-guided SAMs and AAMs.

5.3. Characterization in helicopter infrared

All major military research establishments have developed their own models for prediction of infrared signature level (IRSL) from aircraft. A lot of investigations on predicting infrared signatures for various infrared targets have been made, e.g., exhaust plume[44–46], exhaust nozzle[47–51], aircraft[52–54], etc.

It is known that the temperature distributions on the fuselage skin and in the exhaust plume have a direct impact on infrared signatures of helicopters. Because the temperature distribution on the fuselage skin is governed by heat transfer between the skin and inner hot elements as well as the skin and outer surrounding, there are many factors affecting the temperature distribution, such as rotor downwash, heat radiation from engine casting, convective heat transfer between the skin and cold air, solar irradiance on the skin, etc. On the other hand, the exhaust plume temperature distribution is seriously affected by the rotor downwash flow owing to the mixing action. In order to understand how downwash impacts plume temperature and ejecting capacity of helicopter exhaust systems, Huang et al.[55,56] conducted experimental investigations respectively. In these experiments, the downwash flow was simulated by a low-speed blower and downwash was evenly distributed. While in the modeling of temperature distribution on the helicopter skin, the downwash impact and solar irradiance were not taken into consideration.

Recently, to precisely simulate temperature distributions on the helicopter airframe and in the exhaust plume, the effects of rotor downwash were considered by Pan et al.[57–60] in three-dimensional flow and heat transfer calculation under helicopter hovering. A rotor downwash model was presented to define the external boundary of rotor downwash. Fig. 14 shows the effect of rotor downwash on the exhaust plume. The exhaust plume takes on strong downwards deflection to the rear fuselage, as well as deflection to the rotor's rotational direc-

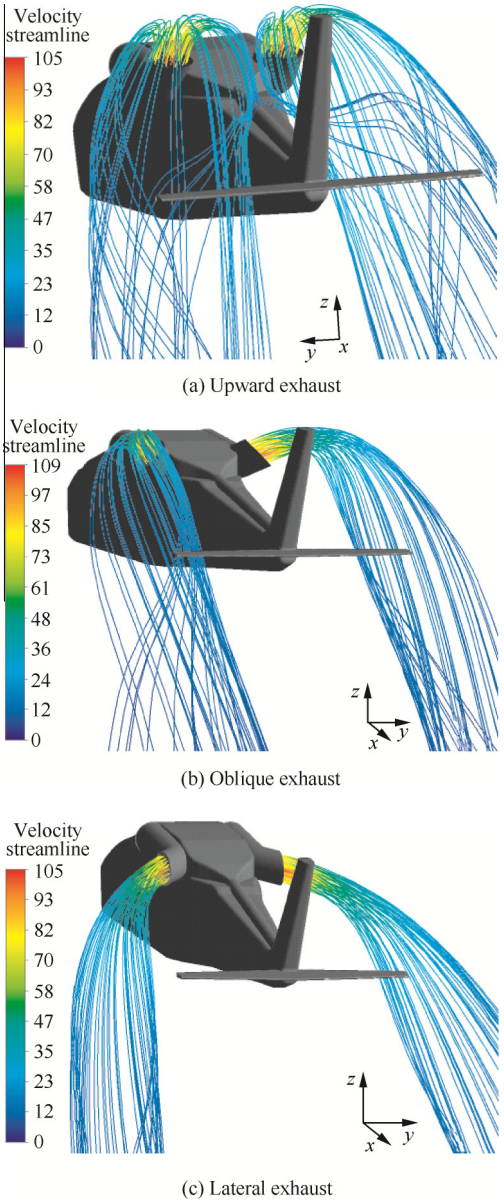

Fig. 14 Plume flow fields (under downwash of 10 m/s).[60]

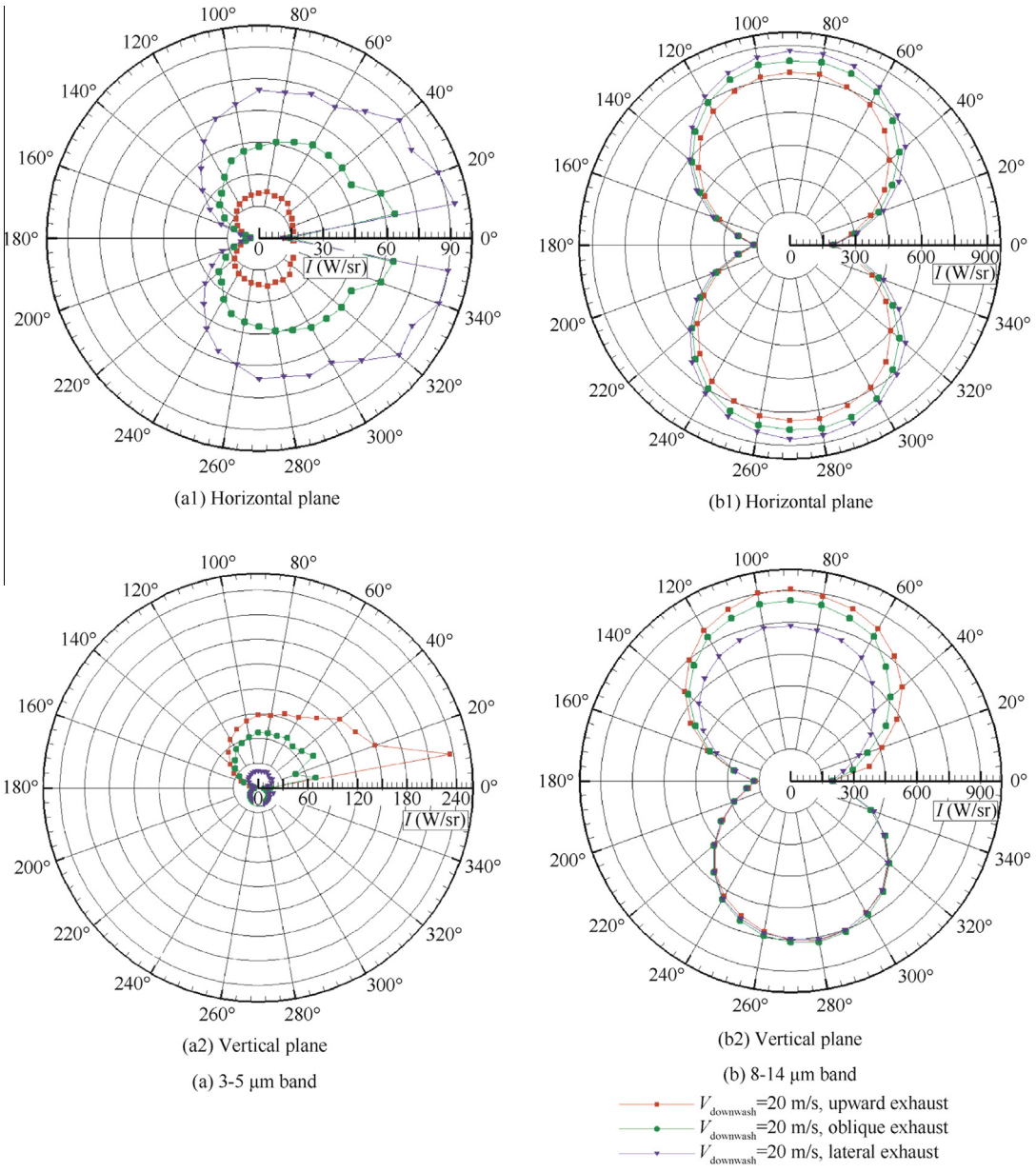

Fig. 15 Infrared intensity in the 3–5 μm and 8–14 μm band under downwash of 20 m/s.[60]

tion, under the action of rotor downwash. These deflections are especially obvious under higher rotor downwash. When the exhaust is ejected upward, the exhaust plume could come into collision with the rear fuselage, and pumping capacity of the exhaust system is weakened a little. While the exhaust is ejected in oblique or lateral directions, the exhaust plumes do not come into collision with the rear fuselage, and pumping capacities of the exhaust system are somewhat enhanced. The exhaust direction shows significant influence on the infrared radiation distribution, as seen in Fig. 15. In this figure, V_{downwash} denotes the downwash velocity. When the exhaust is ejected in the oblique direction, the infrared radiation intensity detected from the top direction is almost the same as that from the lateral direction. While the exhaust is ejected upward or sideward, strong infrared radiation occurs at some viewing directions.

6. Conclusions

Helicopter infrared suppression technology meets very advanced requirements today, but it is also true that it has reached a plateau, for the most part, with further increases in suppressing efficiency, coming as incremental improvements rather than revolutionary changes. In the interim period, advancements in helicopter infrared signature suppression technology have primarily been in more detailed understanding of infrared sources and higher sophistication of analytical tools.

Having reached this plateau, further research on advanced infrared suppression technology is needed in the future. Firstly, the comprehensive infrared suppression in the 3–5 μm and 8–14 μm bands will doubtfully become the emphasis of helicopter stealth. The optimization of emissivity distribution on the fuselage skin is one of important issues. Secondly,

multidisciplinary optimization of a complete infrared suppression system deserves further investigation, such as the utilization of the particle separator air and downwash air to deduce the plume and fuselage temperature. Thirdly, more concise modeling on the helicopter infrared features should be developed taking into consideration of more comprehensive factors, such as the effects of atmospheric transmission and radiance on aircraft infrared signatures, as well as the effects of sunshine, skyshine, and earthshine on aircraft infrared detection.

Acknowledgement

This study was supported by National Level Project and Provincial Level Project.

References

1. Yang YH, Bai CC. The problems of the infrared stealth of the flying vehicles. *Acta Aeronaut Astronaut Sin* 1988;**10**(12):549–54 [Chinese].
2. Paterson J. Overview of low observable technology and its effects on combat aircraft survivability. *J Aircraft* 1999;**36**(2):380–8.
3. Rao GA, Mahulikar SP. New criterion for aircraft susceptibility to infrared guided missiles. *Aerosp Sci Technol* 2005;**9**(8):701–12.
4. Mahulikar SP, Sonawane HR, Rao GA. Infrared signature studies of aerospace vehicles. *Prog Aerosp Sci* 2007;**43**(7):218–45.
5. Thompson J, Birk AM, Cunningham M. Design of infrared signature suppressor for the Bell 205 (UH-1H) helicopters, Part I: aerothermal design. In: *Proceedings of seventh CASI propulsion symposium*; 1999.
6. Barlow B, Petach A. Advanced design infrared suppressor for turbo-shaft engines. In: *Proceedings of the 33rd annual national forum of the American helicopter society*; 1977.
7. Francois T. Internal aerodynamics of infrared suppressors for helicopter engines. *J Am Helicop Soc* 1988;**33**(4):4–14.
8. Mahulikar SP, Prasad HSS, Potnuru SK. Infrared signature suppression of helicopter engine duct based on "conceal and camouflage". *J Propul Power* 2008;**24**(3):613–8.
9. Bettini C, Cravero C, Cogliandro S. Multidisciplinary analysis of a complete infrared suppression system. ASME Paper, GT-2007-27721; 2007.
10. Zhang JZ, Li LG, Gao C, He WB. An experimental study on a lobed nozzle of an infrared suppression system. *J Aerosp Power* 1997;**12**(2):212–4 [Chinese].
11. Zhang JZ, Li LG, Gao C. Model experiments of infrared suppressor for helicopter exhaust system. *J Infrared Millimet Waves* 2005;**24**(2):125–9 [Chinese].
12. Zhang JZ, Shan Y, Li LG. Investigation on lobed nozzle mixer-ejector infrared suppressor for helicopter exhaust system. *Acta Aeronaut Astronaut Sin* 2007;**28**(1):32–6 [Chinese].
13. Shan Y, Zhang JZ. Effect of scale factor on infrared radiation characteristics of helicopter infrared radiation suppressor. *J Aerosp Power* 2008;**23**(2):221–6 [Chinese].
14. Wang TH, Wang XW, Zhang JZ, Shan Y. Effect of covering shelter on infrared radiation characteristics of helicopter infrared radiation suppressor. *J Aerosp Power* 2009;**24**(7):1493–9 [Chinese].
15. Colucci F. Suppressed to survive. *Defen Helicop* 1992;40–5.
16. Kanclebo SW. Boeing Silorsky findings underscore RAH-66 stealth. *AW&ST* 1993;22–3.
17. Tang ZF, Zhang JZ, Shan Y. Investigation on ejecting and mixing characteristics of lobed muzzle with curved mixing duct and slot exit. *J Aerosp Power* 2005;**20**(6):978–82 [Chinese].
18. Tang ZF, Zhang JZ, Wang XW, Liu Q. Experimental research on infrared suppressor integrating the exhaust system with the tail part of a helicopter. *J Aerosp Power* 2007;**22**(2):233–7 [Chinese].
19. Presz WM, Blinn RF, Morin BL. Short efficient ejector systems. AIAA-87-1837; 1987.
20. Presz WM, Morin BL, Gousy RG. Forced mixer lobes in ejector designs. *J Propul Power* 1988;**4**(4):350–5.
21. Paterson RW. Turbofan mixer nozzle flow field-a benchmark experimental study. *J Eng Gas Turbines Power* 1984;**106**(3):692–8.
22. Povinelli LA, Anderson BH. Investigation of mixing in a turbofan exhaust duct. *AIAA J* 1984;**22**(4):518–25.
23. Eckerle JK, Sheibani H, Awad J. Experimental measurement of the vortex development downstream of a lobed forced mixer. *J Eng Gas Turbines Power* 1992;**114**:63–71.
24. McCormick DC, Bennett JC. Vortical and turbulent structure of a lobed mixer free shear layer. *AIAA J* 1994;**32**(9):1852–9.
25. Yu SCM, Yip TH. Experimental investigation of two-stream mixing flows with streamwise and normal vorticity. *Int J Heat Fluid Flow* 1997;**18**(2):253–61.
26. Hu H, Saga T, Kobayashi T, Taniguchi N. A study on a lobed jet mixing flow by using stereoscopic particle image velocimetry technique. *Phys Fluids* 2001;**13**:3425–41.
27. Kozlowski K, Kraft G. Experimental evaluation of exhaust mixers for an energy efficient engine. AIAA-80-1088; 1980.
28. Kuchar AP, Chamberlin R. Scale model performance test investigation of mixed flow exhaust system mixers for an energy efficient engine (E3) propulsion system. AIAA-83-0541; 1983.
29. Skebe SA, Paterson RW, Barber TJ. Experimental investigation of three-dimensional forced mixer lobe flow fields. AIAA-88-3785-CP; 1988.
30. Yu SCM, Yeo JH, Teh JKL. Some measurements downstream of a lobed forced mixer with different trailing edge configurations. *Int Commun Heat Mass Transfer* 1993;**20**(5):721–8.
31. Yu SCM, Hou Y, Chan WK. Scarfing and scalloping effects on lobed forced mixer at low-speed conditions. *J Propul Power* 2000;**16**(3):440–8.
32. Mao R, Yu SCM, Zhou T, Chu LP. On the vorticity characteristics of lobe-forced mixer at different configurations. *Exp Fluids* 2009;**46**(6):1049–66.
33. Salman H, McGuirk JJ, Page GJ. Prediction of a non-isothermal three-dimensional mixing layer created by a scarfed lobed mixer. *Proc Institut Mech Eng Part G J Aerosp Eng* 2006;**220**(5):399–419.
34. Nastase I, Meslem A. Vortex dynamics and mass entrainment in turbulent lobed jets with and without lobe deflection angles. *Exp Fluids* 2010;**48**(4):693–714.
35. Lei ZJ, Mahallati A, Cunningham M, Germain P. Effects of core flow swirl on the flow characteristics of a scalloped forced mixer. *J Eng Gas Turbines Power* 2012;**134**(11): 111201-1-9.
36. Skebe S, McCormick D, Presz W. Parameter effects on mixer-ejector pumping performance. AIAA-88-7018; 1988.
37. Zhang JZ, Shan Y, Li LG. Computation and validation of parameter effects on lobed mixer-ejector performances. *Chin J Aeronaut* 2005;**18**(3):193–8.
38. Liu YH. Experimental and numerical research on high pumping performance mechanism of lobed exhauster-ejector mixer. *Int Commun Heat Mass Transfer* 2007;**34**(2):197–209.
39. Liu YH. Experimental and numerical investigation of circularly lobed nozzle with/without central plug. *Int J Heat Mass Transfer* 2002;**45**(12):2577–85.
40. Shan Y, Zhang JZ. Numerical computation for pumping and mixing performance on mixer-ejector with curved mixing duct. *J Nanjing Univ Aeronaut Astronaut* 2008;**40**(2):137–41 [Chinese].
41. Ponton T, Warnes G. Helicopter IRS engine integration for the "first" technology demonstrator program. ASME Paper, GT-2007-27408; 2007.
42. Presz WM, Werle M. Multi-stage mixer/ejector system. AIAA-2002-4064; 2002.
43. Mahulikar SP, Rao GA, Kolhe PS. Infrared signatures of low-flying aircraft and their rear fuselage skin's emissivity optimization. *J Aircraft* 2006;**43**(1):226–32.

44. Xu NR. Numerical computation on infrared plume radiation. *Acta Aeronaut Astronaut Sin* 1995;**16**(6):647–53 Chinese.
45. Heragu SS, Rao KVL, Raghunandan BN. Generalized model for infrared perception from an engine exhaust. *J Thermophys Heat Transfer* 2002;**16**(1):68–76.
46. Mahulikar SP, Rao GA, Sane SK. Aircraft plume modelling for infrared signature studies. *Int J Turbo Jet Engin* 2011;**28**(3):187–97.
47. Rao GA, Mahulikar SP. Aircraft powerplant and plume infrared signature modelling and analysis. AIAA-2005-0221; 2005.
48. Wang HL, Zhang JZ, Shan Y. Numerical study on infrared radiation characteristics of spherical convergent flap nozzles. *Acta Aeronaut Astronaut Sin* 2009;**30**(9):1576–82 [Chinese].
49. Yang CY, Zhang JZ, Shan Y. Numerical simulation on infrared radiation characteristics of single expansion ramp nozzles. *Acta Aeronaut Astronaut Sin* 2010;**31**(10):1919–26 [Chinese].
50. Zhang SL, Shan Y, Zhang JZ, Zhang Y. Research on the aerodynamic and infrared radiation characteristics of single expansion ramp vector nozzle. *Acta Aeronaut Astronaut Sin* 2012;**33**(8):1406–16 [Chinese].
51. Huang W, Ji HH. Computational investigation of infrared radiation characteristics of exhaust system based on BRDF. *Acta Aeronaut Astronaut Sin* 2012;**33**(7):1227–35 [Chinese].
52. Mahulikar SP, Sane SK, Gaitonde UN, Marathe AG. Numerical studies of infrared signature levels of complete aircraft. *Aeronaut J* 2001;**1046**(105):185–92.
53. Rao GA, Mahulikar SP. Effect of atmospheric transmission and radiance on aircraft infrared signatures. *J Aircraft* 2005;**42**(4):1046–54.
54. Lu JW, Wang Q. Aircraft-skin infrared radiation characteristics modeling and analysis. *Chin J Aeronaut* 2009;**22**(5):493–7.
55. Zhu Y, Huang Y. Experimental investigation of exit temperatures of an infrared suppressor model. *J Aerosp Power* 2007;**22**(7):1142–7 [Chinese].
56. Wang XW, Huang Y, Lu YX. Influences of the downwash flow from a helicopter rotor on the performances of an infrared suppressor. *J Aerosp Power* 2003;**18**(6):772–6 [Chinese].
57. Pan CX, Zhang JZ, Shan Y. Modeling and analysis of helicopter skin temperature distributions. *Acta Aeronaut Astronaut Sin* 2011;**32**(2):249–56 [Chinese].
58. Pan CX, Zhang JZ, Shan Y. Modeling and analysis of helicopter thermal and infrared radiation. *Chin J Aeronaut* 2011;**24**(5):558–67.
59. Pan CX, Zhang JZ, Shan Y. Effects of exhaust temperature on helicopter infrared signature. *Appl Therm Eng* 2013;**51**:529–38.
60. Pan CX, Zhang JZ, Ren LF, Shan Y. Effects of rotor downwash on exhaust plume flow and helicopter infrared signature. Applied Thermal Engineering [accepted].

Zhang Jingzhou is a professor, born in 1964, he received B.S. degree from Tsinghua University in 1986 and M.S. degree from Southeast University in 1989 and Ph.D. degree from Nanjing University of Aeronautics and Astronautics in 1992 respectively. He has done a lot of researches on mixer-ejector and enhanced heat transfer, and published approximately 200 scientific papers in various periodicals.